Manara
Qatar Research
Repository
by Qatar National Library

First principles investigation of CO and CO2 adsorption on graphene nanoribbon modified by ZrOx

Ahmad I. Ayesh

Item type
Journal Contribution

Terms of use
This work is licensed under a CC BY 4.0 license

This version is available at
https://manara.qnl.qa/articles/journal_contribution/First_principles_investigation_of_CO_and_CO_sub_2_sub_adsorption_on_gra
Access the item on Manara for more information about usage details and recommended citation.

Posted on Manara – Qatar Research Repository on
2023-11-01

Diamond & Related Materials 139 (2023) 110371

Contents lists available at ScienceDirect

Diamond & Related Materials

journal homepage: www.elsevier.com/locate/diamond

First principles investigation of CO and CO_2 adsorption on graphene nanoribbon modified by ZrO_x

Ahmad I. Ayesh *

Physics Program, Department of Mathematics, Statistics and Physics, College of Arts and Sciences, Qatar University, P.O. Box 2713, Doha, Qatar

ARTICLE INFO

Keywords:
DFT
First-principles
Graphene nanoribbon
Gas sensors
Metal oxide
ZrO_x
CO
CO_2

ABSTRACT

Carbon dioxide (CO_2) is normally emitted from anthropogenic and natural sources, and it is a greenhouse gas that is directly linked to climate change. CO is a main sink of OH molecules in the troposphere to produce CO_2. Precise evaluation of the concentrations of the two gases is essential for controlling their emission. The influence of Armchair-graphene nanoribbon (GNR) modification by ZrO_x (where $x = 0, 1, or\ 2$) on its adsorption of CO and CO_2 is inspected in this investigation. First principles computations that employ density functional theory (DFT) are utilized to assess gas adsorption by evaluation of the adsorption energy (E_{ga}) and length (D), exchange of charge between the gas and the structure (ΔQ_T), density of states (DOS), along with the band structure. The modification of GNR is established by atomic substitution (doping) or deposition on GNR structure (decoration). The results indicate outstanding enhancement of CO and CO_2 adsorption on the modified GNR structures. However, doping is more efficient than decoration for adsorption of both gases. In particular, the Zr doped GNR has the highest capacity for both gases' adsorption, where the adsorption energy for CO and CO_2 increases 18.4 and 16.5 times, respectively, reference to the pristine GNR. The outcomes of this investigation promote the utilization of ZrO_x doping of GNR as an approach for the fabrication of highly sensitive and selective environmental CO and CO_2 sensors.

1. Introduction

Emission of carbon dioxide (CO_2) is a major factor that is responsible for greenhouse effect, and it is directly linked to climate change [1]. This gas can be emitted through anthropogenic and natural sources including energy and agriculture sectors [2]. CO_2 is known of its major impact on climate change globally due to its high radiative forcing (around 1.82 W/m^2) and atmospheric lifetime [3,4]. On the other hand, carbon monoxide (CO) is not a greenhouse gas but it has a noteworthy contribution to the tropospheric chemistry [5]. CO is mainly produced in the troposphere through oxidation of CH_4 using OH, along with other pathways including incomplete processes of combustion. Additionally, CO is the main sink of OH molecules in the troposphere to produce CO_2. Consequently, the link between CO and CO_2 chemistry is well established and accurate measurements of their concentrations are essential to understand their tropospheric reactions. Production of precise CO/CO_2 monitoring devices enables accurate monitoring and control of their emission.

Detection of CO/CO_2 can be established using conductometric sensors where adsorption of a gas on a functional material modifies its electrical conductance. The functional materials can be designed by doping or decoration using suitable materials to make them selective to particular gases [6]. The utilization of CO/CO_2 sensors is essential for human safety especially in locations with high gas emission concentration where it is required to evaluate environment quality [7]. The sensor detection signal is sent to control systems that apply safety programed actions [8].

Two dimensional nanostructure of carbon atoms with a honeycomb atomic arrangement is known as graphene [9]. It is a material of unique characteristics including the outstanding optical transparency as well as thermal conduction. Its high atomic density limits its gas penetration [10]. Graphene can be categorized based on its atomic arrangement into zigzag, that is known as a conductor, and armchair that may be either conductor or semiconductor [11,12]. Herein, armchair-graphene is a semiconductor when the number of dimers is $3i$ or $3i+1$, while it is a metal when the number is $3i+2$ (i = integer) [13]. The band gap of graphene can be controlled by reducing graphene dimensions to quasi or one dimension in a form of graphene nanoribbon (GNR), i.e. decreasing

* Corresponding author.
E-mail address: ayesh@qu.edu.qa.

https://doi.org/10.1016/j.diamond.2023.110371
Received 13 June 2023; Received in revised form 3 September 2023; Accepted 3 September 2023
Available online 9 September 2023
0925-9635/© 2023 The Author. Published by Elsevier B.V. This is an open access article under the CC BY license (http://creativecommons.org/licenses/by/4.0/).

the width of GNR will increase the band gap [14]. GNR is utilized widely for devices in multiple fields such as biodevices, chemical sensors, optical devices, etc. [15,16]. The ability of GNR to adsorb large number of gases make it ideal for utilization for gas sensor applications [16]. Yet, GNR must to be modified using an appropriate approach (doping, defect, decoration of the surface, …) to adjust its selectivity to particular gases [17,18]. Furthermore, vacancy generation in GNR is expected to create new adsorption sites for gases.

GNR has been investigated intensively recently for gas and chemical sensor utilization, and its efficiency has been demonstrated in many labs [19,20]. V. Naganaboina et al. reported CO gas sensors using CeO_2 modified graphene nanoplatelets that are functional at room temperature and could detect concentrations as low as 9 ppm [21]. Graphene oxide sheets were produced by heating that yielded deoxygenation and generation of reduced graphene oxide [22]. The sensors had high detection limit of 10 nM concentration, and the incorporation of SnO_2 improved the detection limit for CO_2 by ~50 %. E. Salih et al. investigated CO and CO_2 adsorption on GNR modified by epoxy and hydroxyl groups computationally and reported enhancement of their adsorption [23]. The Pt doped GNR was examined for CO and CO_2 adsorption by DFT computations and an enhancement was demonstrated in the adsorption by 9 times as compared with the pristine structure [24]. Graphene of double vacancy modified by transition metals was examined for gas sensing, and the results demonstrated that the Fe and Co modified structures were suitable for CO and CO_2 sensing [25]. However, the effect of ZrO_x modification of GNR on its adsorption for CO and CO_2 was not examined, yet, it is well known of its high reaction with CO and CO_2 [26].

The impact of modifying GNR (*number of dimers* = $3i$) by ZrO_x (where $x = 0, 1, or\ 2$) on its CO/CO_2 adsorption capacity is evaluated using first-principles DFT-computations in this work. GNR is modified by two pathways: doping (central carbon atoms are replaced by ZrO_x), and decoration (positioning ZrO_x on a central point at GNR surface). ZrO_x is selected in this work due to its high adsorption capacity to CO_x, especially in nanoparticle form [27].

The capacity of CO/CO_2 adsorption on the modified and unmodified GNR structures is assessed through investigation of density-of-states (DOS), band structure modification, transfer of charge, as well as adsorption length and energy.

2. Computational method

The computations were performed using a Virtual-Nanolab (VNL) software package form Synopsys. The VNL involved a simulation platform: Quantum Atomistic toolkit (ATK). Kohn-Sham method of DFT computation was utilized to examine the adsorption of CO and CO_2 gases on ZrO_x modified GNR. GNR was modified using ZrO_x where it was either substituted carbon atoms (doping), or placed on the surface of GNR (decoration). The new structures are presented in Table 1. Pseudopotential perturbation associated with linear-collection of atomic orbitals (LCAO) were employed as a framework of this work. The electrons were modeled for each structure as a system of non-interacting gas with an effective potential energy ($V_{ef}(n)$) that can be expressed as [28]:

$$V_{ef}(n) = V_H(n) + V_{exch}(n) + V_s(n) \quad (1)$$

where n indicated the density of electrons, $V_H(n)$ was the Hartree potential for the interaction between electrons, $V_{exch}(n)$ was the potential of exchange-correlation, and $V_s(n)$ was the electrostatic potential of electrons.

The Kohn-Sham Hamiltonian ($\widehat{H}_{KS}$) was indicated as [28]:

$$\widehat{H}_{KS} = -\frac{\hbar^2}{2m}\nabla^2 + V_{ef}(n) \quad (2)$$

where m was the electron mass, while the $\hbar = \frac{h}{2\pi}$ was the reduced constant of Planck (h was the Planck's constant). The Kohn-Sham Hamiltonian was executed using the DFT-LCAO computations by utilizing numerical values that enabled effective execution of the calculations for GNR structures. Local-density approximations (LDA) as well as generalized-gradient approximations (GGA) were realized. Electron exchange and correlation were included using the formalism of Perdew–Burke–Ernzerhof (PBE) incorporated with Grimme (DFT—D2) approximations [29]. The utilized formalism involved the effect of Van der Waals force which enabled accurate and efficient DFT computations [30,31]. It should be noted that the spin effect is not considered in the computations since the presented structure is polarized: electrons in graphene are not spin polarized and in GNR, and ZrO_x is not a magnetic martials [32]. Furthermore, all computations were performed at a temperature of 300 K, where increasing the temperature might increase the kinetic energy of gases and reduce the probability of their adsorption.

The edges of all investigated pristine and modified GNR structures were terminated using hydrogen atoms to reduce their edge effect [33]. Next, the GNR structures were modified by ZrO_x (ZrO_x denotes to Zr, ZrO, or ZrO_2) using two pathways: i) doping where ZrO_x replaced central carbon atoms, and ii) decoration where ZrO_x was placed on a central location of the GNR surface. It should be noted that the ZrO_x modification of GNR was made at a central point to reduce the effect of dangling bonds. All GNR structures were optimized beforehand any computations by a package within the ATK-VNL software: LBFGS [34]. Additionally, each structure was relaxed to maximum force-per-atom and stress tolerance of $0.05\ eV/\text{Å}$ and $0.1 GPa$, respectively. The GNR structures were constructed at $4 \times 2 \times 1$ k-point with 100 Hartree density for mesh sampling. The gas adsorption energy (E_{ga}) on a GNR structure was evaluated using [23]:

$$E_{ga} = E_{GNR+CO_x} - (E_{GNR} + E_{CO_x}) \quad (3)$$

where E_{GNR+CO_x} was the total energy of GNR with the gas adsorbed (for CO_x, $x = 1\ or\ 2$), E_{GNR} was total energy of GNR without adsorption, and E_{CO_x} was the gas total energy. Accordingly, the suitability of a structure for CO/CO_2 adsorption could be evaluated based on the value of adsorption energy. Herein, the strongest adsorption was assigned to the lowest negative value of E_{ga}. Furthermore, the capacity of a structure for gas adsorption was assessed by evaluation of the charge transferred between CO/CO_2 and a GNR structure. The charge transferred could be assessed by Mulliken population using [35]:

$$\Delta Q_T = q_f - q_0 \quad (4)$$

where q_0 and q_f were the original and final charges, respectively, of the CO/CO_2 gas. A positive value of ΔQ_T designated that charges were transferred from GNR to CO/CO_2 gas.

Table 1
Energy band gaps of the pristine and modified structures prior to CO/CO_2 adsorption. The ZrO_x-on-GNR notation is used for decorated structures, while the ZrO_x + GNR notation is used for the doped structures.

Structure	E_g (eV)
GNR	0.7122
Zr-on-GNR	0.2516
ZrO-on-GNR	0.4404
ZrO_2-on-GNR	0.2471
Zr + GNR	0.4596
ZrO + GNR	0.0775
ZrO_2 + GNR	0.0579

3. Results and discussion

Pristine GNR structure is constructed and modified at a central location to minimize the edge effect of using ZrO_x as presented in Fig. 1. The carbon atoms of the pristine GNR structure have a symmetrical arrangement with a C—C bond length between 1.42 and 1.43 Å. The figure reveals that doping (Fig. 1(b)–(d)) changes the structure of carbon atoms around the doping cite. All atoms of ZrO_x establish bonds with carbon atoms within the GNR structure. Slight reorganization of carbon atoms is observed as a result of energy optimization nearby the doping site. Furthermore, no dramatic change in the structure of atoms (such as reconstruction) due to the satisfaction of the dangling bonds at the edges by hydrogen atoms [33]. Decoration (Fig. 1(e)–(g)) has less effect than doping on the structure of carbon atoms. Both Zr and ZrO establish bonds with GNR structure at interstitial positions. However, no bond is observed for the case of ZrO_2 that can be assigned to its higher degree of chemical stability (compared with both Zr and ZrO) [36].

The lengths of bonds of the ZrO_x - GNR within the doped structures are: 1.90 Å of the C—Zr in the Zr + GNR structure; 1.90 Å for O—Zr, 1.42–1.44 Å for O—C, and 1.86–1.87 Å for C—Zr in the ZrO + GNR structure; and 1.89 Å for O—Zr, 1.42–1.44 Å for O—C, 1.83 Å for C—Zr in the ZrO_2 + GNR. The lengths of bonds of the ZrO_x - GNR within the decorated structures are: 2.30 Å for C—Zr in the Zr-on-GNR structure; 1.78 Å for O—Zr and 2.41–2.44 Å for C—Zr in the ZrO-on-GNR structure; and 1.82 Å for O—Zr and 2.75–2.95 Å for C—Zr in the ZrO_2-on-GNR structure. The adjustment of bond length of O—Zr, C—Zr, and C—O following to GNR modification with ZrO_x is assigned to the stress relief after bonding [37].

The band gaps of the ZrO_x modified GNR structures are evaluated as presented in Table 1. The pristine GNR structure exhibit the maximum value of band gap energy. In general, the doped GNR structures have lower band gap energies than the decorated ones, where the lowest band gaps are observed for the ZrO and ZrO_2 doped GNR structures.

The band structure variation as a result of modification of GNR by ZrO_x is presented in Fig. 2. Each band structure has a parabolic shape around the Γ-point. Herein, the symmetry around the Γ-point is considered since it exhibits the lowest band gab energy. Higher DOS within conduction as well as valance bands can be observed for modified structures as compared with the pristine one. The band structures contain the projections of the different orbitals, however, the manuscript focuses on the main structure since it serves the objective of this work. The modification shifts the valance band adjacent to the Fermi level and generates additional bands close to it, in agreement with the results presented in Table 1.

Fig. 3 shows the optimized pristine and modified GNR structures post to CO adsorption. The figure illustrates that CO is unbonded to all pristine and decorated GNR structures, while it is bonded to all doped ones. The bonds are established to ZrO_x cite in the doped GNR structures. Furthermore, a chemical bond is established only between CO and ZrO_2 in the decorated structure but without any connection to GNR. Upon introduction of CO, it reorients itself during the optimization process to minimize the structure total energy and hence stabilizes it. It can be stated that chemisorption of CO on the doped GNR is a favorable adsorption unlike both pristine and decorated GNR. Fig. 4 presents the GNR structures post to CO_2 adsorption. The figure illustrates that CO_2 is chemisorbed only on the Zr doped GNR structure, while no chemisorption occurs for the pristine, ZrO-doped, ZrO_2-doped, and all decorated structures. Figs. 3 and 4 demonstrate that adsorption of CO and CO_2 is favorable on the doped GNR structures but less favorable on both pristine as well as decorated GNR structures.

The band structure variation as a result of CO and CO_2 adsorption on pristine and modified GNR structures is presented in Figs. 5 and 6, respectively. The figures show that new bands are generated upon modification and gas adsorption. Generally, adsorption of the gas increases the band gap. Adsorption of CO_2 on a GNR structure increases its band gap such that it is larger than its equivalent upon CO adsorption. The band gap values of GNR structures after adsorption of CO and CO_2 gases are presented in Table 2. The alteration of the band structure as well as generation of new bands post to CO and CO_2 adsorption illustrate the introduction of additional electronic states because of the gas adsorption [38]. The adjustments in the band gap together with the introduction of new bands demonstrate that the ZrO_x modification of GNR is an effective approach to enhance its adsorption for CO and CO_2 gases. The increase in the band gap energy can be assigned to the competition between the Coulomb attraction of the gas and ZrO_x species, and correlation by charges of nonbonding states [39]. The DOS of pristine and ZrO_x modified GNR structures post adsorption of CO and CO_2 as compared with the unexposed pristine GNR is presented in Fig. 7. The figure demonstrates that the DOS of pristine and modified GNR is generally lower than that of the unexposed pristine GNR. Doping of GNR by ZrO_x and exposure to CO and CO_2 cause generation of new electronic bands within the conduction band, valance band, and band gap. For example, the DOS intensity of pristine GNR increases after adsorption of CO at the bands 2.62 and −3.72 eV, and after adsorption of CO_2 at the bands 3.71 and −4.53 eV. New bands are generated for the Zr doped GNR after adsorption of CO at the bands 3.97, −1.72, and −3.82 eV, and

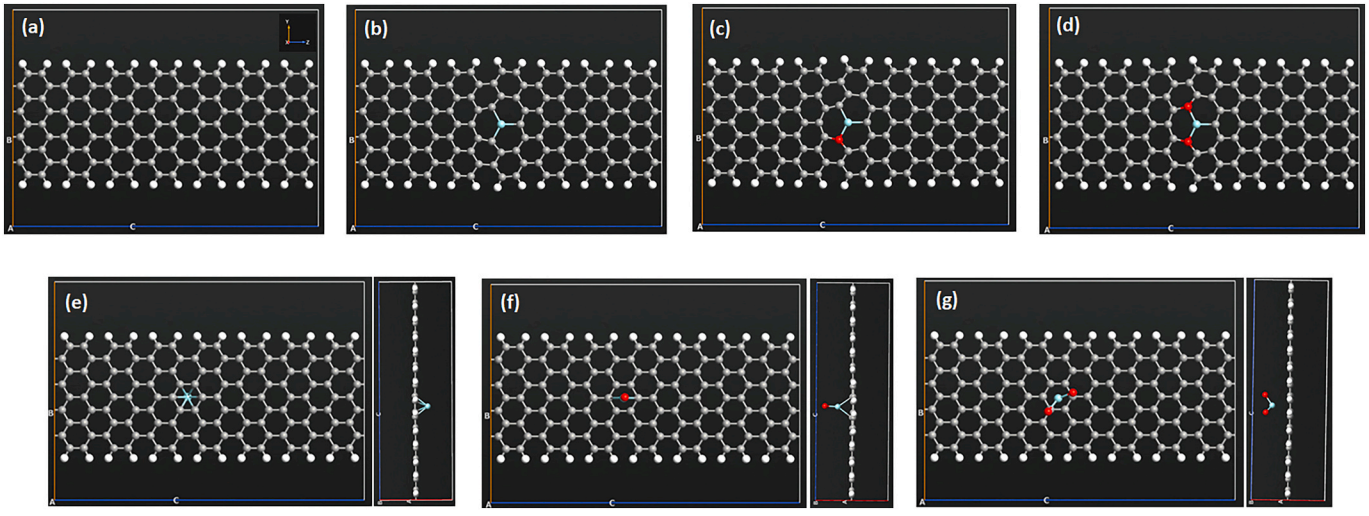

Fig. 1. The optimized GNR structures prior to gas adsorption of pristine GNR (a), doped (b–d), and decorated structures (e–g). b) Zr + GNR, c) ZrO + GNR, d) ZrO_2 + GNR, e) Zr-on-GNR, f) ZrO-on-GNR, and g) ZrO_2-on-GNR.

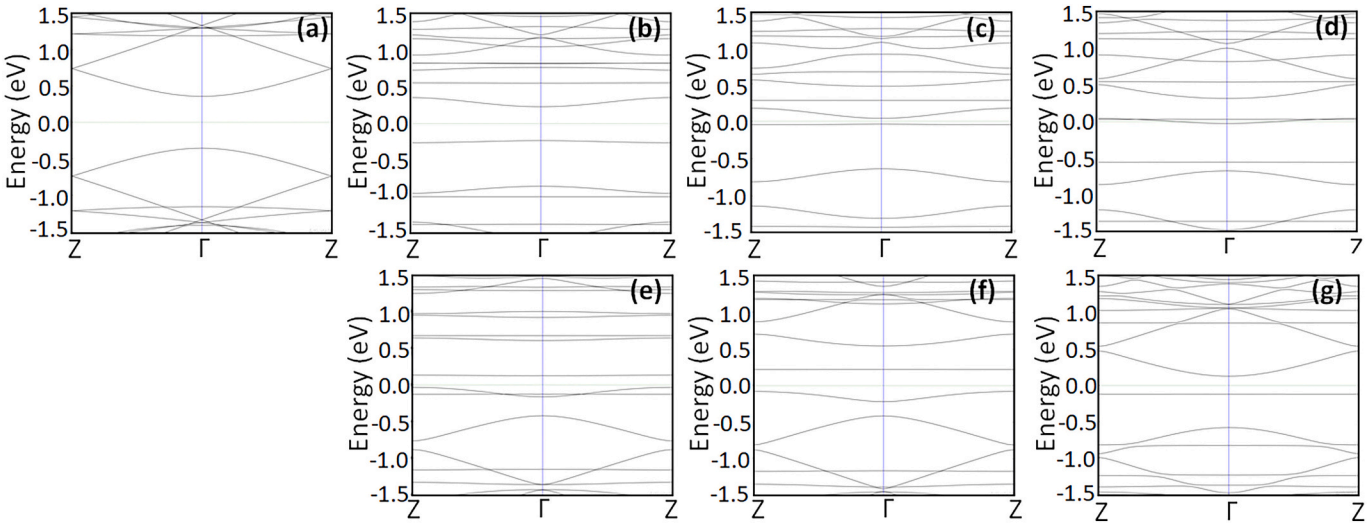

Fig. 2. The band diagrams of the optimized pristine and modified GNR structures prior to gas adsorption: a) pristine GNR, b) Zr + GNR, c) ZrO + GNR, d) ZrO_2 + GNR, e) Zr-on-GNR, f) ZrO-on-GNR, and g) ZrO_2-on-GNR.

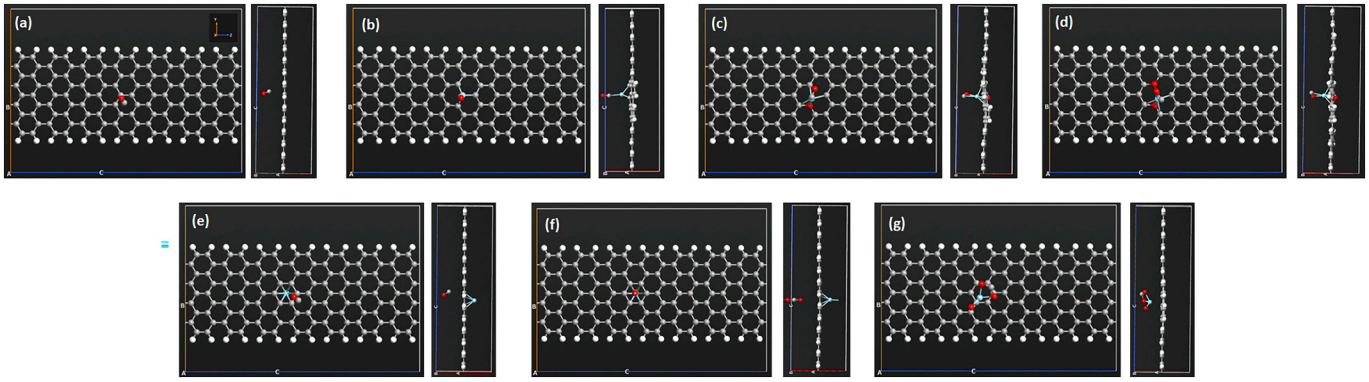

Fig. 3. The optimized GNR structures post to CO adsorption of pristine GNR (a), doped (b–d), and decorated structures (e–g). b) Zr + GNR, c) ZrO + GNR, d) ZrO_2 + GNR, e) Zr-on-GNR, f) ZrO-on-GNR, and g) ZrO_2-on-GNR.

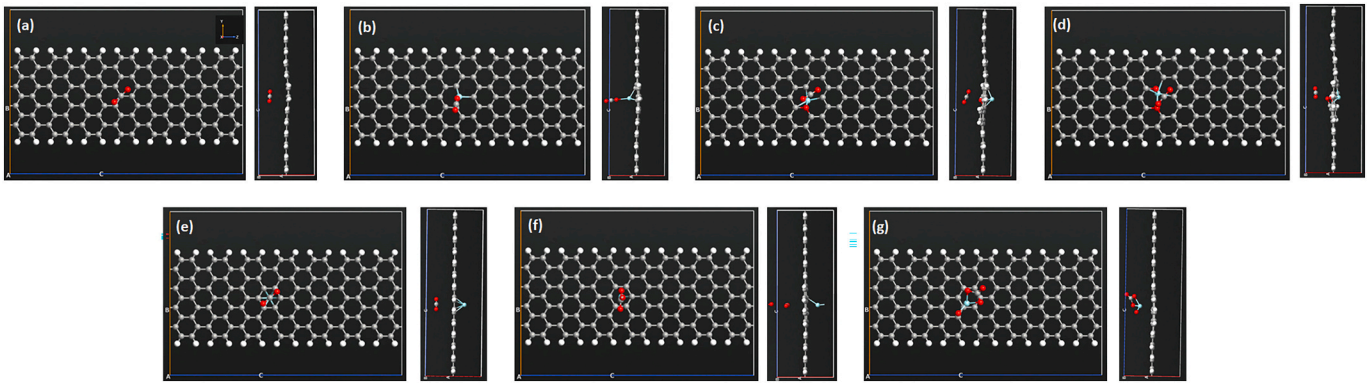

Fig. 4. The optimized GNR structures post to CO_2 adsorption of pristine GNR (a), doped (b–d), and decorated structures (e–g). b) Zr + GNR, c) ZrO + GNR, d) ZrO_2 + GNR, e) Zr-on-GNR, f) ZrO-on-GNR, and g) ZrO_2-on-GNR.

after adsorption of CO_2 at the bands −1.72 and −3.82 eV. New bands are generated for the ZrO doped GNR after adsorption of CO at the bands 0.73 and −0.16 eV, and after adsorption of CO_2 at the bands 3.42 and −0.16 eV. New bands are generated for the ZrO_2 doped GNR after adsorption of CO at the bands 2.10 and −0.51 eV, and after adsorption of CO_2 at the bands 2.02 and −0.51 eV. Bands at different locations are generated for the decorated structure after gas adsorption, for instance, the bands at −0.09, −0.07, and 2.49 eV are generated after CO adsorption on the Zr, ZrO and ZrO_2 doped GNR (respectively), while the bands at −0.09, 0.57, and −0.97 eV are generated after CO_2 adsorption on the Zr, ZrO and ZrO_2 doped GNR (respectively). Fig. 7 shows that the DOS of modified GNR after exposure to CO and CO_2 increases around the Fermi level, in agreement with the observations of Figs. 2, 5, and 6. The general features of DOS for the pristine and ZrO_x modified GNR after

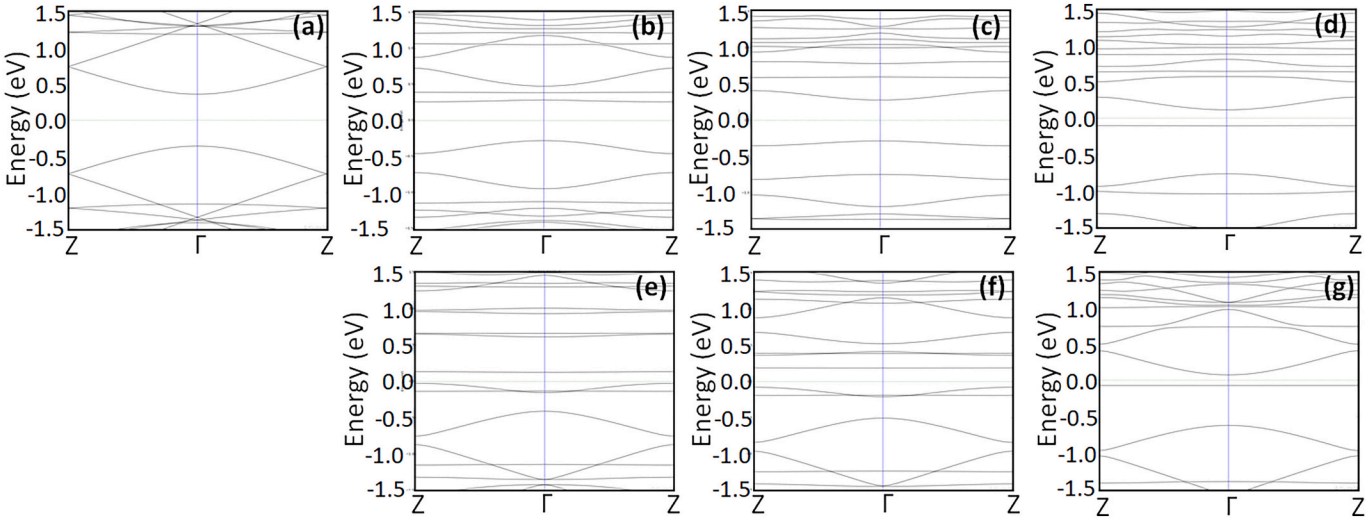

Fig. 5. The band diagrams of the optimized pristine and modified GNR structures post to CO adsorption: a) pristine GNR, b) Zr + GNR, c) ZrO + GNR, d) ZrO_2 + GNR, e) Zr-on-GNR, f) ZrO-on-GNR, and g) ZrO_2-on-GNR.

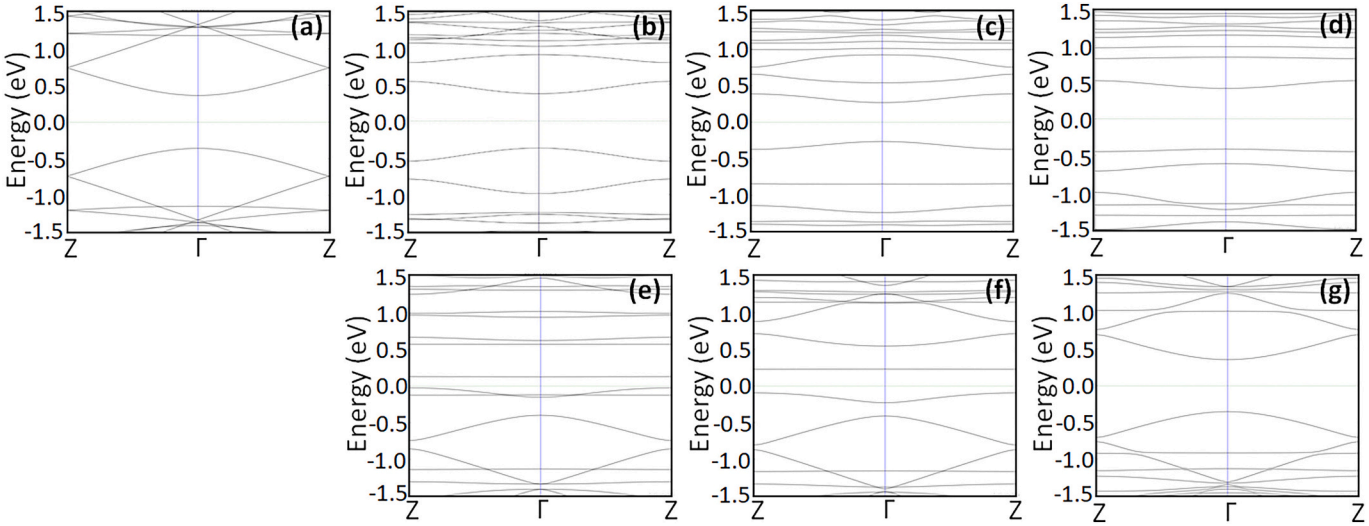

Fig. 6. The band diagrams of the optimized pristine and modified GNR structures post to CO_2 adsorption: a) pristine GNR, b) Zr + GNR, c) ZrO + GNR, d) ZrO_2 + GNR, e) Zr-on-GNR, f) ZrO-on-GNR, and g) ZrO_2-on-GNR.

Table 2
Calculated parameters of the pristine and modified structures post to CO/CO_2 adsorption: energy band gap (E_g), adsorption energy (E_{ga}) and length (D), along with charge transferred (ΔQ_T).

Structure	E_g (eV)	E_{ga} (eV)	D (Å)	ΔQ_T (e)
CO + GNR	0.7147	−0.4901	3.0200	−0.0090
CO + Zr-on-GNR	0.2586	−0.5211	2.9000	−0.0100
CO + ZrO-on-GNR	0.3750	0.3194	3.7900	−0.2870
CO + ZrO_2-on-GNR	0.1472	−1.9060	2.6300	0.3300
CO + Zr + GNR	0.5637	−9.0231	2.3600	−0.0240
CO + ZrO + GNR	0.5635	−8.5311	2.3400	0.1970
CO + ZrO_2 + GNR	0.2219	−8.6503	2.2900	0.3380
CO_2 + GNR	0.7224	−0.5015	3.2800	0.0070
CO_2 + Zr-on-GNR	0.2442	−0.4360	3.4700	0.0040
CO_2 + ZrO-on-GNR	0.4595	−0.5934	3.5900	0.2500
CO_2 + ZrO_2-on-GNR	0.7074	−2.5815	3.2400	0.5680
CO_2 + Zr + GNR	0.7375	−8.2607	2.3600	−0.1010
CO_2 + ZrO + GNR	0.5327	−7.5749	3.1200	0.0050
CO_2 + ZrO_2 + GNR	0.8292	−8.8558	2.9300	0.0480

exposure to CO and CO_2 are symmetrical to those of pristine unexposed GNR. Additional electronic states are introduced for the ZrO_x modified GNR after exposure to CO and CO_2 [40]. Therefore, ZrO_x modification of GNR can be considered as an effective methodology for CO and CO_2 gas adsorption.

The capacity of the pristine and ZrO_x modified GNR for CO and CO_2 is assessed by evaluation of the adsorption energy as illustrated in Table 2. The table reveals clear enhancement of E_{ga} of adsorption of CO and CO_2 for GNR as a result of ZrO_x modification. The doped GNR structures adsorb both CO and CO_2 more effectively than the decorated ones. The highest adsorption energy of CO gas is for the Zr doped GNR (−9.0231 eV), while the highest adsorption energy of CO_2 gas is for the ZrO_2 doped GNR (−8.8558 eV). However, the capacity of the GNR structures for adsorption of CO and CO_2 can be evaluated by combining the adsorption energy results with the observations in Figs. 3 and 4. CO is physically combined with all doped GNR structures, yet, CO_2 is only bonded with the Zr doped GNR structure. This structure has a relatively high adsorption energy for CO_2 (−8.2607 eV), hence, it can be highlighted as the structure with the highest capacity for CO_2 adsorption. Therefore, the Zr doped GNR structure is the structure of the best

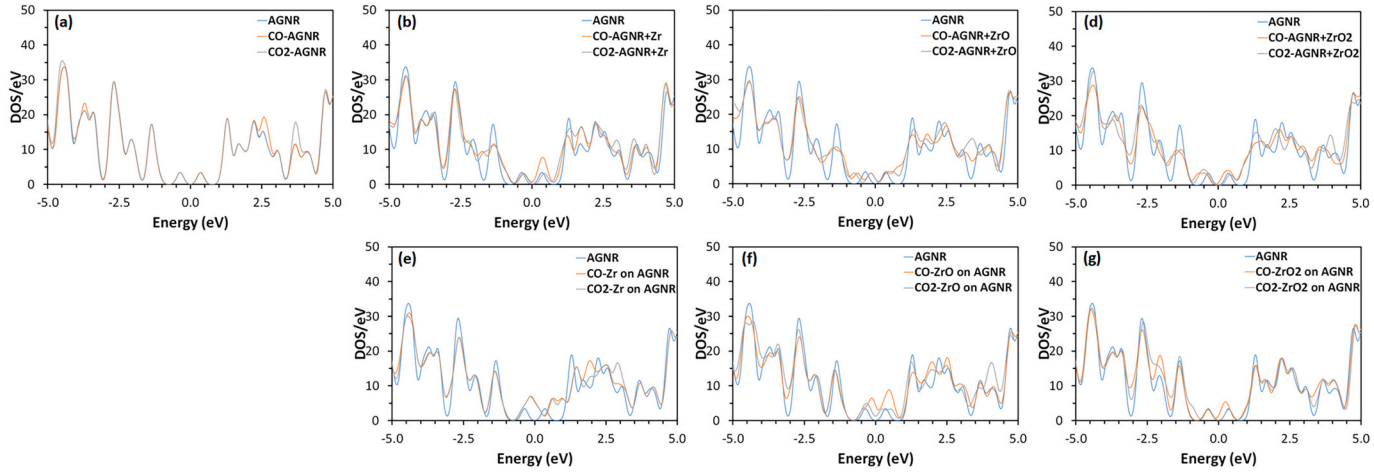

Fig. 7. Density of states of the optimized pristine and modified GNR structures prior and post CO/CO_2 adsorption for: a) pristine GNR, b) Zr + GNR, c) ZrO + GNR, d) ZrO_2 + GNR, e) Zr-on-GNR, f) ZrO-on-GNR, and g) ZrO_2-on-GNR.

adsorption capacity for both gases with the highest adsorption energy for CO. The low values of adsorption energies for CO and CO_2 on pristine GNR (−0.4901 and −0.5015, respectively) indicate their unfavorable adsorption. The CO and CO_2 adsorption energies on the Zr doped GNR are 18.4 and 16.5 times, respectively, higher reference to the pristine GNR. A comparison between the adsorption energies evaluated in this work with recently reported values for graphene-based structures is presented in Table 3. The table presents that an excellent enhancement has been achieved in this work for adsorption of CO and CO_2 through Zr doping.

The adsorption length is evaluated by measuring the bond length between the gas and GNR structure and it can be used to assess the capacity of gas adsorption. A small adsorption length points to the robust adsorption of the gas on a structure. Table 2 shows that the Zr doped GNR structure has a low adsorption energy for both CO and CO_2 (2.36 Å for both) in agreement with the high magnitude of adsorption energy of this structure for both gases. The pristine GNR in addition to the decorated structures (for the case of CO_2 gas) exhibit large adsorption lengths signifying their small adsorption capacity. The ZrO_2 doped GNR structure also exhibits low adsorption length for CO in agreement with its relatively high adsorption energy. The low adsorption length for CO on the ZrO_2 decorated GNR is misrepresentative since no chemical bond exists between the gas and the structure. The adsorption energy of CO on the ZrO decorated GNR is positive indicating that gases have unfavorable adsorption which is in agreement with the observation in Fig. 3(f). The table also shows the charge transferred between the gases and GNR structures. The charge density difference diagrams of pristine and modified structures before and after adsorption of CO and CO_2 gases are shown in the Supplementary Fig. S1. The figure shows the charge density difference in color code: blue is negative, while pink is positive. High charge density difference is associated with the structures with high charge transfer (for example, CO_2 adsorbed on ZrO_2 on GNR). The value of the charge is negative for both CO and CO_2 on the Zr doped GNR structure indicating that charge is transferred from the gas to the structure. Additionally, ΔQ_T has the lowest negative value for both gases on the Zr doped GNR (except for CO on the ZrO decorated GNR, however, the gas here is not attached to the structure). The noticeable values of ΔQ_T transferred from CO and CO_2 to the Zr doped GNR agree with their large adsorption energies and low adsorption lengths. Furthermore, this also is in agreement with the chemisorption of gases observed in Figs. 3 and 4. The observed negative charge transferred from CO and CO_2 to the Zr doped GNR justify the introduction of new electronic bands after adsorption as observed in Figs. 5 and 6, and thus, the robust adsorption of the gases on the structure [41]. The values of ΔQ_T for both gases on pristine GNR are low (compared with that of the Zr doped GNR) in agreement with the observation that the gases are not chemisorbed on the structure.

Table 3
Reported adsorption energies of CO/CO_2 on graphene based structures.

Structure	E_{ga}(CO) (eV)	E_{ga}(CO_2) (eV)	Reference
Zr doped GNR	−9.0231	−8.2607	This work
Pt doped armchair graphene nanoribbon	−5.967	−4.014	[24]
O and OH modified armchair graphene nanoribbon	−0.303	−0.538	[23]
Graphyne	−0.139	−0.188	[52]
Ir modified graphene with single vacancy	−1.79		[53]
Fe doped graphene		−1.5	[54]

CO gas has a high adsorption energy with the observed chemisorption on all ZrO_x doped GNR structures with minor differences. However, CO_2 is chemisorbed and has high adsorption energy on the Zr doped GNR structure only. Therefore, the Zr doped GNR can be considered as a suitable structure for both CO and CO_2 adsorption. The adsorption energy values of CO and CO_2 on this structure are 1.5 and 2.0, respectively, times higher than those reported for them on Pt doped GNR [24]. The evaluated values of the adsorption energy and length indicate that the ZrO_x doped GNR structures are more favorable for CO than the decorated structures. For CO_2, the only favorable structure is the Zr doped GNR [42–44]. Accordingly, doping GNR with ZrO_x is a more efficient approach for CO and CO_2 adsorption than decoration. The improvement of CO and CO_2 adsorption on GNR upon doping with ZrO_x is assigned to its high affinity to both gases [36,45]. The excellent adsorption of CO is allocated to its oxidation to CO_2 due to oxidative adsorption that is promoted by ZrO_x [46]. The GNR doping by ZrO_x promotes its reactivity because of the contribution of additional negative charges into the delocalized π-bond that result from the larger electronegativity of ZrO_x within the GNR-doped structures when compared to the pristine one [37]. Additionally, the less favorable adsorption of CO and CO_2 on decorated GNR is assigned to the lower hybridization that occurs in the overlapped electronic orbitals of carbon (2p) as well as zirconium (both 3d and 4s) [47]. The orbitals of carbon, zirconium, and oxygen (2p, 3d, and 2p, respectively) within the doped GNR structures have sturdy hybridization [47]. The decent adsorption of CO on ZrO_x can be assigned to the close C—O bond that is adjacent to the CO gas gas-phase [48]. As for CO_2, electron transfer generates a surface carbonate by the oxide anion, O^{2-}, to the anti-bonding π level in CO_2 [48]. Thanks for the redox-cycle as well as the superior surface acidity that enable excellent reactivity of

CO and CO_2 reduction. The adsorption of CO on ZrO_x however is more efficient due to the formation of CO_2 that is more stable [49]. This can be illustrated according to the below equations where CO adsorb electrons to the ZrO_X [50]:

$$O_2 + CO \rightarrow O_{2-adsorbed} + CO_2 \quad (5)$$

$$O_{2-adsorbed} + CO \rightarrow CO_2 \quad (6)$$

CO_2 also is adsorbed on ZrO_x trough reaction with oxygen ion:

$$CO_{2(adsorbed)} + O^-_{2(adsorbed)} + 2e^- \rightarrow CO^-_{2(adsorbed)} + 2O^-_{(adsorbed)} \quad (7)$$

This reaction generates extra charges as presented in Table 2. For the decorated structures, ZrO_x utilizes its bonds for bonding with GNR, hence, CO and CO_2 have relatively low affinity for bonding with the structures as a result of chemical bond satisfaction.

Fabrication of environmental monitoring gas sensors for CO and CO_2 can benefit from the advances in their adsorption on the ZrO_x modified GNR. The gas sensor response (SR) is given by:

$$SR = \left| \frac{\rho_f - \rho_0}{\rho_0} \right| \quad (8)$$

Here, ρ_0 and ρ_f are the resistivities of the structure prior and post exposure to the gas, respectively. The sensor resistivity may be assessed by [51]:

$$\rho_{(0\ or\ f)} = De^{\frac{E_{g\ (0\ or\ f)}}{2k_BT}} \quad (9)$$

In the equation, D is a constant (pre-exponential that is temperature independent), T is the GNR temperature, $E_{g\ (0\ or\ f)}$ is the estimated energy of the band gap prior and post gas adsorption (respectively), while the Boltzmann constant k_B is 8.62×10^{-5} eV.K^{-1}. The outcome of Eq. (9) is a qualitative value of the resistivity based on the computations, while the precise value is found experimentally. Hence, the evaluated sensor response is also an estimated value. The sensor response of pristine GNR upon exposure to CO is 0.05 while it increases to 6.48 for the Zr doped GNR. Those values indicate a large enhancement of the response due to Zr doping of GNR as well as the suitability of ZrO_x doped GNR for CO adsorption. Additionally, the result is in agreement with the evaluated values of E_{ga}, D, and ΔQ_T in Table 2. Consequently, doping of GNR by ZrO_x can be considered for applications of environmental CO and CO_2 gas sensors, with the best sensitivity of both gases for the Zr doped GNR.

4. Conclusion

Armchair-graphene nanoribbon (GNR) has been explored in the last decade for implementation as a sensitive material for environmental gas sensors, yet, its modification is necessary to promote the selectivity for particular gases. The effect of modifying GNR by ZrO_x (ZrO_x is Zr, ZrO, or ZrO_2) on its adsorption for CO and CO_2 gases is examined in this work. First principles computations that employ density functional theory (DFT) are utilized to assess gas adsorption by evaluation of the adsorption energy (E_{ga}) and length (D), exchange of change between the gas and the structure (ΔQ_T), density of states (DOS), along with the band structure. GNR is modified using ZrO_x either by atomic substitution (doping) or deposition on GNR structure (decoration). The outcomes reveal that ZrO_x modification of GNR greatly enhances its CO and CO_2 adsorption. In particular, doping is more efficient than decoration for both gas adsorption. Additionally, Zr doped GNR has the highest capacity for both gases adsorption. Yet, the Zr doped GNR exhibits higher adsorption energy for CO than CO_2. The adsorption energy of the Zr doped GNR for CO and CO_2 increases 18.4 and 16.5 times, respectively, reference to the pristine GNR. Therefore, ZrO_x doping of GNR may be applied for the fabrication of highly sensitive and selective environmental CO and CO_2 sensors.

Supplementary data to this article can be found online at https://doi.org/10.1016/j.diamond.2023.110371.

CRediT authorship contribution statement

Ahmad I. Ayesh: Visualization, Investigation, Writing – original draft, Conceptualization, Methodology, Software, Supervision, Writing – review & editing.

Declaration of competing interest

The authors declare that they have no known competing financial interests or personal relationships that could have appeared to influence the work reported in this paper.

Data availability

Data will be made available on request.

Acknowledgments

Open Access funding provided by the Qatar National Library.

References

[1] S. Fawzy, A.I. Osman, J. Doran, D.W. Rooney, Strategies for mitigation of climate change: a review, Environ. Chem. Lett. 18 (2020) 2069–2094.
[2] A.K. Patra, Trends and projected estimates of GHG emissions from Indian livestock in comparisons with GHG emissions from world and developing countries, Asian Australas. J. Anim. Sci. 27 (2014) 592.
[3] E. Dlugokencky, S. Houweling, chemistry of the atmosphere|methane, in: G. R. North, J. Pyle, F. Zhang (Eds.), Encyclopedia of Atmospheric Sciences (Second Edition), Academic Press, Oxford, 2015, pp. 363–371.
[4] Z. Xiong, Z. Liang, Y. Bu, K. Li, H. Zhang, J. Zhang, The effect of vacancy size on the oxidation process of graphene by CO2: a ReaxFF molecular dynamics study, Diam. Relat. Mater. 136 (2023), 109989.
[5] L. Smoydzin, P. Hoor, Contribution of Asian emissions to upper tropospheric CO over the remote Pacific, Atmos. Chem. Phys. 22 (2022) 7193–7206.
[6] A.I. Ayesh, H2S and SO2 adsorption on Cu doped MoSe2: DFT investigation, Phys. Lett. A 422 (2022), 127798.
[7] F. Niu, Z.-W. Shao, H. Gao, L.-M. Tao, Y. Ding, Si-doped graphene nanosheets for NOx gas sensing, Sensors Actuators B Chem. 328 (2021), 129005.
[8] Z. Felegari, S. Hamedani, Adsorption properties of the phosgene molecule on pristine graphyne, BN-and Si-doped graphynes: DFT study, Results Phys. 7 (2017) 2626–2631.
[9] P.R. Wallace, The band theory of graphite, Phys. Rev. 71 (1947) 622.
[10] S.M. Mariappan, M.K. Eswaran, U. Schwingenschlögl, T. Thangeeswari, E. Vinoth, M. Shkir, Z. Said, B. Karthikeyan, Impact of reducing agents on the ammonia sensing performance of silver decorated reduced graphene oxide: experiment and first principles calculations, Appl. Surf. Sci. 558 (2021), 149886.
[11] I. Ahmadi, F. Khoeini, Highly tunable charge transport in defective graphene nanoribbons under external local forces and constraints: a hybrid computational study, Results Phys. 20 (2021), 103770.
[12] X. Li, X. Wang, L. Zhang, S. Lee, H. Dai, Chemically derived, ultrasmooth graphene nanoribbon semiconductors, Science 319 (2008) 1229–1232.
[13] Y.-W. Son, M.L. Cohen, S.G. Louie, Energy gaps in graphene nanoribbons, Phys. Rev. Lett. 97 (2006), 216803.
[14] E. Salih, A.I. Ayesh, Enhancing the sensing performance of zigzag graphene nanoribbon to detect NO, NO2, and NH3 gases, Sensors 20 (2020) 3932.
[15] P.V. Barkov, O.E. Glukhova, Carboxylated graphene nanoribbons for highly-selective ammonia gas sensors: ab initio study, Chemosensors 9 (2021) 84.
[16] A.I. Ayesh, Effect of CuOx additive site to graphene nanoribbon on its adsorption for hydrogen sulfide, Results Phys. 24 (2021), 104199.
[17] H.-p. Zhang, X.-g. Luo, X.-y. Lin, X. Lu, Y. Leng, Density functional theory calculations of hydrogen adsorption on Ti-, Zn-, Zr-, Al-, and N-doped and intrinsic graphene sheets, Int. J. Hydrog. Energy 38 (2013) 14269–14275.
[18] H. Tang, Y. Xiang, H. Zhan, Y. Zhou, J. Kang, DFT investigation of transition metal-doped graphene for the adsorption of HCl gas, Diam. Relat. Mater. 136 (2023), 109995.
[19] A.I. Ayesh, R.E. Ahmed, M.A. Al-Rashid, R.A. Alarrouqi, B. Saleh, T. Abdulrehman, Y. Haik, L.A. Al-Sulaiti, Selective gas sensors using graphene and CuO nanorods, Sensors Actuators A Phys. 283 (2018) 107–112.
[20] A.I. Ayesh, Z. Karam, F. Awwad, M.A. Meetani, Conductometric graphene sensors decorated with nanoclusters for selective detection of Hg2+ traces in water, Sensors Actuators B Chem. 221 (2015) 201–206.
[21] V.R. Naganaboina, S.G. Singh, Graphene-CeO2 based flexible gas sensor: monitoring of low ppm CO gas with high selectivity at room temperature, Appl. Surf. Sci. 563 (2021), 150272.
[22] N.S. Singh, F. Mayanglambam, H.B. Nemade, P. Giri, Facile synthetic route to exfoliate high quality and super-large lateral size graphene-based sheets and their applications in SERS and CO 2 gas sensing, RSC Adv. 11 (2021) 9488–9504.

[23] E. Salih, A.I. Ayesh, CO, CO2, and SO2 Detection Based on Functionalized Graphene Nanoribbons: First Principles Study, Physica E: Low-Dimensional Systems and Nanostructures, 2020, p. 114220.
[24] E. Salih, A.I. Ayesh, Pt-doped armchair graphene nanoribbon as a promising gas sensor for CO and CO2: DFT study, Phys. E. 125 (2021), 114418.
[25] A. Baby, C. Di Valentin, Gas sensing by metal and nonmetal co-doped graphene on a Ni substrate, J. Phys. Chem. C 125 (2021) 24079–24095.
[26] P.G. Patil, D. Kajale, V. Patil, G. Patil, G. Jain, Synthesis of nanostructured ZrO 2 for gas sensing application, Int. J. Smart Sens. Intell. Syst. 5 (2012).
[27] Y.H. Wang, W.G. Gao, H. Wang, Y.E. Zheng, W. Na, K.Z. Li, Structure–activity relationships of Cu–ZrO 2 catalysts for CO 2 hydrogenation to methanol: interaction effects and reaction mechanism, RSC Adv. 7 (2017) 8709–8717.
[28] S. Smidstrup, T. Markussen, P. Vancraeyveld, J. Wellendorff, J. Schneider, T. Gunst, B. Verstichel, D. Stradi, P.A. Khomyakov, U.G. Vej-Hansen, QuantumATK: an integrated platform of electronic and atomic-scale modelling tools, J. Phys. Condens. Matter 32 (2019), 015901.
[29] J.P. Perdew, K. Burke, M. Ernzerhof, Generalized gradient approximation made simple, Phys. Rev. Lett. 77 (1996) 3865.
[30] S. Grimme, Semiempirical GGA-type density functional constructed with a long-range dispersion correction, J. Comput. Chem. 27 (2006) 1787–1799.
[31] E. Salih, A.I. Ayesh, First principle study of transition metals codoped MoS2 as a gas sensor for the detection of NO and NO2 gases, Phys. E (2021) 114736.
[32] N. Kheirabadi, A. Shafiekhani, The ground state of graphene and graphene disordered by vacancies, Phys. E. 47 (2013) 309–315.
[33] T. Kawai, Y. Miyamoto, O. Sugino, Y. Koga, Graphitic ribbons without hydrogen-termination: electronic structures and stabilities, Phys. Rev. B 62 (2000) R16349.
[34] D.C. Liu, J. Nocedal, On the limited memory BFGS method for large scale optimization, Math. Program. 45 (1989) 503–528.
[35] E. Salih, A.I. Ayesh, Pt-doped armchair graphene nanoribbon as a promising gas sensor for CO and CO2: DFT study, Phys. E (2020) 114418.
[36] E.I. Kauppi, K. Honkala, A.O.I. Krause, J.M. Kanervo, L. Lefferts, ZrO2 acting as a redox catalyst, Top. Catal. 59 (2016) 823–832.
[37] Z. Khodadadi, Evaluation of H2S sensing characteristics of metals–doped graphene and metals-decorated graphene: insights from DFT study, Phys. E. 99 (2018) 261–268.
[38] V.E.C. Padilla, M.T.R. de la Cruz, Y.E.Á. Alvarado, R.G. Díaz, C.E.R. García, G. H. Cocoletzi, Studies of hydrogen sulfide and ammonia adsorption on P-and Si-doped graphene: density functional theory calculations, J. Mol. Model. 25 (2019) 94.
[39] S. Yu, W. Zheng, C. Wang, Q. Jiang, Nitrogen/boron doping position dependence of the electronic properties of a triangular graphene, ACS Nano 4 (2010) 7619–7629.
[40] G.K. Walia, D.K.K. Randhawa, First-principles investigation on defect-induced silicene nanoribbons—a superior media for sensing NH3, NO2 and NO gas molecules, Surf. Sci. 670 (2018) 33–43.
[41] T. Zhang, H. Sun, F. Wang, W. Zhang, S. Tang, J. Ma, H. Gong, J. Zhang, Adsorption of phosgene molecule on the transition metal-doped graphene: first principles calculations, Appl. Surf. Sci. 425 (2017) 340–350.
[42] T. Pakornchote, A. Ektarawong, B. Alling, U. Pinsook, S. Tancharakorn, W. Busayaporn, T. Bovornratanaraks, Phase stabilities and vibrational analysis of hydrogenated diamondized bilayer graphenes: a first principles investigation, Carbon 146 (2019) 468–475.
[43] M.G. Ahangari, A.H. Mashhadzadeh, M. Fathalian, A. Dadrasi, Y. Rostamiyan, A. Mallahi, Effect of various defects on mechanical and electronic properties of zinc-oxide graphene-like structure: a DFT study, Vacuum 165 (2019) 26–34.
[44] X. Gao, Q. Zhou, J. Wang, L. Xu, W. Zeng, Adsorption of SO2 molecule on Ni-doped and Pd-doped graphene based on first-principle study, Appl. Surf. Sci. 146180 (2020).
[45] H. Okamoto, H. Obayashi, T. Kudo, Carbon monoxide gas sensor made of stabilized zirconia, Solid State Ionics 1 (1980) 319–326.
[46] M. Machida, A. Yoshii, T. Kijima, Temperature swing adsorption of NOx over ZrO2-based oxides, Int. J. Inorg. Mater. 2 (2000) 413–417.
[47] E. Mohammadi-Manesh, M. Vaezzadeh, M. Saeidi, Cu-and CuO-decorated graphene as a nanosensor for H2S detection at room temperature, Surf. Sci. 636 (2015) 36–41.
[48] H.-Y.T. Chen, S. Tosoni, G. Pacchioni, A DFT study of the acid–base properties of anatase TiO2 and tetragonal ZrO2 by adsorption of CO and CO2 probe molecules, Surf. Sci. 652 (2016) 163–171.
[49] D.C. da Silva, S. Letichevsky, L.E. Borges, L.G. Appel, The Ni/ZrO2 catalyst and the methanation of CO and CO2, Int. J. Hydrog. Energy 37 (2012) 8923–8928.
[50] M.D. Esrafili, N. Saeidi, Sn-embedded graphene: an active catalyst for CO oxidation to CO2? Phys. E. 74 (2015) 382–387.
[51] T. Liu, Z. Cui, X. Li, H. Cui, Y. Liu, Al-doped MoSe2 monolayer as a promising biosensor for exhaled breath analysis: a DFT study, ACS Omega 6 (2020) 988–995.
[52] F. Mofidi, A. Reisi-Vanani, Investigation of the electronic and structural properties of graphyne oxide toward CO, CO2 and NH3 adsorption: a DFT and MD study, Appl. Surf. Sci. 507 (2020), 145134.
[53] A. AkÇA, O. Karaman, C. Karaman, N. Atar, M.L. Yola, A comparative study of CO catalytic oxidation on the single vacancy and di-vacancy graphene supported single-atom iridium catalysts: a DFT analysis, Surf. Interfaces 25 (2021), 101293.
[54] J. Ni, M. Quintana, S. Song, Adsorption of small gas molecules on transition metal (Fe, Ni and Co, Cu) doped graphene: a systematic DFT study, Phys. E. 116 (2020), 113768.